CAVITATION DAMAGE IN PARTICLE-LADEN LIQUIDS WITH CONSIDERING PARTICLE CONCENTRATION AND SIZE

KUNPENG SU
College of Water Conservancy and Hydropower Engineering, Hohai University, Nanjing, China, kunpengsu@yahoo.com

JIANHUAWU
College of Water Conservancy and Hydropower Engineering, Hohai University, Nanjing, China, jhwu@hhu.edu.cn

DINGKANG XIA
College of Water Conservancy and Hydropower Engineering, Hohai University, Nanjing, China, xiadingkang@hhu.edu.cn

ZHIYU DING
College of Water Conservancy and Hydropower Engineering, Hohai University, Nanjing, China, island555@163.com

ABSTRACT

Although the main properties of solid particles that influence cavitation erosion in particle-laden liquids have been extensively studied, the mechanisms behind the part that solid particles play remain poorly understood, and little work has been done to clearly identify the relationship between the erosive wear and particle size or concentration. Cavitation erosion of AISI 1045 carbon steel was studied in the presence of SiO_2 microparticles suspended in transformer oil, and 5 diameters (10 μm, 25 μm, 60 μm, 85 μm, and 100 μm) were investigated over a range of concentrations (0.005 v/v, 0.01 v/v, 0.02 v/v, 0.05 v/v, 0.1 v/v and 0.2 v/v). The test results indicate that material removal gets more severe at low concentrations and is reduced at high concentrations; at moderate concentrations, the large particles aggravate erosion while small ones mitigate. Possible influencing mechanisms at given particle sizes and particle concentrations have also been proposed.

Keywords: Cavitation erosion, particle suspensions, particle size, particle concentration, viscosity

1. INTRODUCTION

Chute spillways suffer from cavitation erosion as well as sand abrasion, and the synergistic effect is complex. Although much research in recent years (Hou et al., 2020; Romero et al., 2019; Stella et al., 2019; Lian et al., 2018; Gou et al., 2018) has focused on this synergistic effect, opinions differ on the role solid particles play.

Early investigators assumed that the rough surface of solid particles provides additional nucleation sites for the formation of cavitation bubbles (Harvey et al., 1944), contributing to a decrease in the cavitation threshold. This hypothesis might be verified by the enhancement of sonochemical yields in the presence of suspended solids (Stoian et al., 2018). Over the past two decades, microscopic interactions between a solid particle and a collapsing bubble adjacent or attached to it have been visualized with the aid of high-speed photography (Teran et al., 2019; Zhang et al., 2016; Borkent et al., 2008; Ohl et al., 2004). Before striking a solid surface, the particle can be significantly accelerated away during bubble collapse or rebound. It was also envisaged that particles in adequate quantities could modify liquids' macroscopic properties such as viscosity (Einstein, 1906; Krieger and Dougherty, 1959; Mueller et al., 2010), shielding the surface from the destructive effects of impinging particles or micro-jets, akin to the cushioning effect of air bubbles (Wu et al., 2017), which makes the synergism even more complicated.

Among numerous factors influencing cavitation erosion in particle suspensions (CE_P), particle properties such as shape, hardness, density, size and concentration have also generated considerable research interest over the past two decades. Chen et al. (2007) revealed that irregularly-shaped particles (5 μm, 0.2 wt%) can make indentations in the solid surface and cause higher surface roughness than spherical ones do, though particle shape has little to do with the number of collapsing vapor bubbles. Their team also observed reduced CE_P with increasing diameters (d_p from 0.30-23.34 μm) and volume fractions (φ_p from 1-10 mg/L) (Chen et al., 2009), yet again confined to dilute suspensions of small spherical SiO_2 particles. Hu and Zheng (2017) reported a rise in CE_P as φ_p of large sharp-edged sands (152 μm, 3-10 wt%) increases, despite an initial reduction in CE_P at low φ_p (0.5-3 wt%) and a slight decrease in roughness when φ_p exceeds 5 wt%. Wu and Gou (2013) noticed a clear distinction between small river-sand particles (26-43 μm) and large ones (63-531 μm) with respect to the influence of φ_p (25-85 kg/m^3) on CE_P, as further validated by Wang et al. (2018), and their study suggested a critical size of near 50 μm when CE in sand-free water would be equal to CE_P.

Although previous research has more or less taken into account these main properties of solid particles in investigating CE_P, little has been done to identify the relationship between CE_P and particle characteristics (concentration and size), to the exclusion of potential influences of other physical properties. The purpose of the present paper is to investigate the effect of particle concentration and size (excluding the effect of particle shape) on several parameters relating to CE_P based on orthogonally designed experiments.

2. EXPERIMENTAL FACILITIES AND MATERIALS

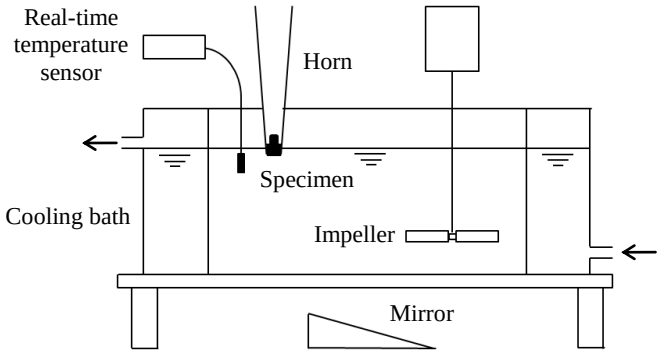

Figure 1. Schematic diagram of the experimental set-up

The experimental configuration is shown schematically in Fig. 1. Cavitation erosion tests were conducted with a piezoelectric vibration device (VCY-1500, Shanghai Y&Y Sonic) operating at 20±0.5 kHz. The replaceable specimen threaded in the horn tip was axially oscillated with a peak-to-peak amplitude of 50±2.5 μm. Its test surface was immersed to a depth of 2 mm in solid-liquid mixtures, with which a cylindrical Perspex vessel (R = 100 mm) was filled to a height of 100 mm. The liquid temperature in the vicinity of specimen surface was maintained at 25±1 ℃ by means of a cooling bath and monitored using a real-time temperature sensor. During the tests, solid particles were kept in suspension using an eccentrically located 75-mm-diameter four-bladed impeller as the agitator, whose relative off-bottom clearance and shaft eccentricity were set equal to 25% and 55%, respectively. The impeller and the horn tip were placed symmetrically around the axis of the vessel. All tests were performed at the critical impeller speeds required to 'just suspend' all solids off the vessel bottom, predetermined based on the criterion proposed by Zwietering (1958).

All specimens, stored in desiccators when not being tested, were machined out of AISI 1045 carbon steel with its chemical composition (wt%) of C: 0.45%, Cr: 0.20%, Mn: 0.65%, Ni: 0.25%, P: 0.03%, S: 0.03% and Si: 0.25%. Its density and Brinell hardness were 7.85×10^3 kg/m^3 and 163 HB, respectively. The test surface of each specimen was ground and polished to an average surface roughness of 20 nm prior to tests.

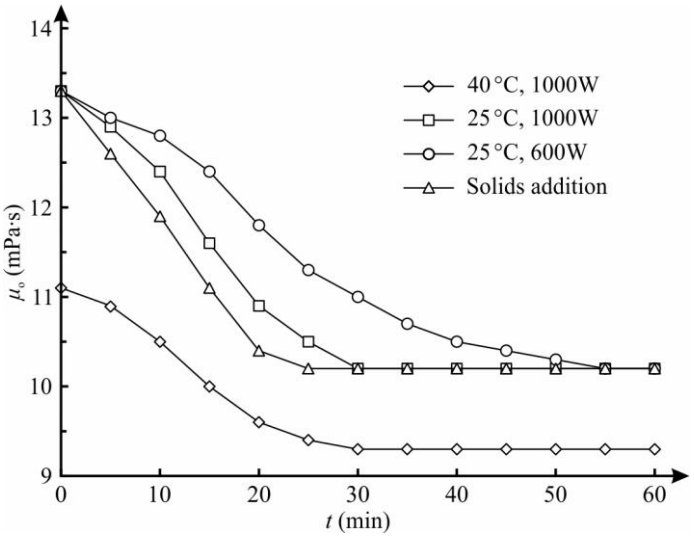

Figure 2. Variation of oil viscosity reduction with temperature, output power and solids addition

Monodisperse non-porous SiO_2 microspheres of five diameters (d_p) were purchased from Shanghai Aladdin Biochemical Technology Co., Ltd. (10 μm, 25 μm and 85 μm) and Tokyo Chemical Industry Co., Ltd. (60 μm and 100 μm), and were used as received. The density and purity of these SiO_2 micro-particles are 2.55×10^3 kg/m^3 and 99.7% (trace metals basis), respectively. To investigate the effects of particle concentration (φ_p) on CE_P, we varied φ_p in the range of 0.005-0.2 v/v, that is, 0.005 v/v, 0.01 v/v, 0.02 v/v, 0.05 v/v, 0.1 v/v and 0.2

v/v. Transformer oil (Type II, supplied by Sunoco Lubricants), instead of ionized water or vegetable oils, was selected as the liquid phase due to its agreeable viscosity (13.3 mPa s at 25 ℃) and oxidation stability. Its specific gravity and interfacial tension at 25 ℃ were 0.887 and 51×10^{-3} N/m, respectively.

Since the production of highly reactive free-radical species during cavitational process can lead to oxidative scission of C-C bonds in long-chain alkenes and thus a decrease in oil viscosity (Mercantili et al., 2015), the effect of sonication on the viscosity of transformer oil (μ_o) was determined. Fig. 2 gives its viscosity change with increasing sonication time for 60 min at different liquid temperatures (25 ℃ and 40 ℃), different output powers (600 W and 1000 W) and with/without the addition of SiO_2 particles (25 μm, 0.02 v/v). The samples of oil were all sonicated for a series of 5 min intervals, and a digital rotational viscometer (NDJ-5S) provided readings of their viscosities with a margin of error of 0.1 mPa s (0.2%FS). It is clearly shown that the steady-state viscosity of fully sonicated transformer oil depends simply on temperature, while power intensities and the presence of solids merely alter the decreasing rate of oil viscosity. Given this fact, to reach its steady-state post-sonication viscosity (10.2 mPa s at 25 ℃), all transformer oil used in cavitation erosion tests had to undergo a half-hour presonication process, followed by immediate removal of sludge as the inevitable by-product of oil oxidation.

The testing of each specimen was continued for a total of 300 min, although the specimen was removed every 15 min (for the first hour) or 30 min to measure the mass lost. Shorter intervals near the beginning of tests contribute to more accurate establishment of erosion-time curves in the early stages. Mass loss was divided by the density of the material to obtain the volume loss, which in turn was divided by total surface area to determine the mean depth of erosion (*MDE*). At the beginning and after each test period, the specimen was washed, air-dried and weighed with an analytical balance (0.1 mg readability). Considering oil deterioration and particle size reduction (Lu et al., 2002) after sonication, the mixture was replaced every hour. Each test was repeated 3 times and the average values are used in subsequent analyses.

3. RESULTS AND DISCUSSION

3.1 In the absence of SiO_2 particles

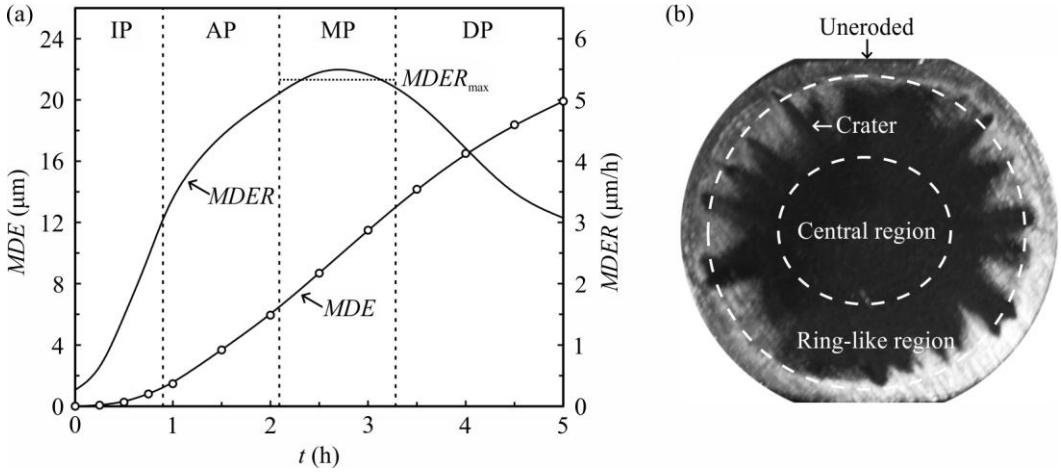

Figure 3. (a) *MDE-t* and *MDER-t* curves and (b) specimen surface at t = 300 min for the solids-free case

The variation of *MDE* with time t in solids-free transformer oil, using a B-spline curve for data fitting, is presented in Fig. 3(a), where the evolution of mean-depth-of-erosion rates (*MDER*) are also given as the first derivative of the *MDE-t* curve. The erosion rate is generally time-dependent and, as expected, the curve can be divided into four characteristic stages: incubation period (IP, assumed in this paper as the period when *MDE* does not exceed 1.0 μm), acceleration period (AP), maximum-rate period (MP) and deceleration period (DP). We define the MP as the period when the absolute rate of change of *MDER* with respect to time is no more than 1 μm/h per hour, and the maximum erosion rate $MDER_{max}$ as the average value of *MDER* during the MP by means of the mean value theorem for integrals. It appears to be approaching a steady-state erosion rate following the DP.

In the absence of SiO_2 particles, as can be seen from Fig. 3(a), the IP lasts for approximately 50 min and $MDER_{max}$ is 5.4 μm/h over the MP (from 125-200 min). The cumulative *MDE* at the conclusion of the test, MDE_{5h}, reaches 19.8 μm when deep radial craters (in a ring-like region) can be found on the specimen surface, which is also dotted with small pits (in the elliptical central region), as presented in Fig. 3(b). The erosion at the outermost perimeter is virtually negligible, mainly due to the central distribution of cavitation bubbles during high frequency oscillations of the horn.

3.2 In the presence of SiO_2 particles

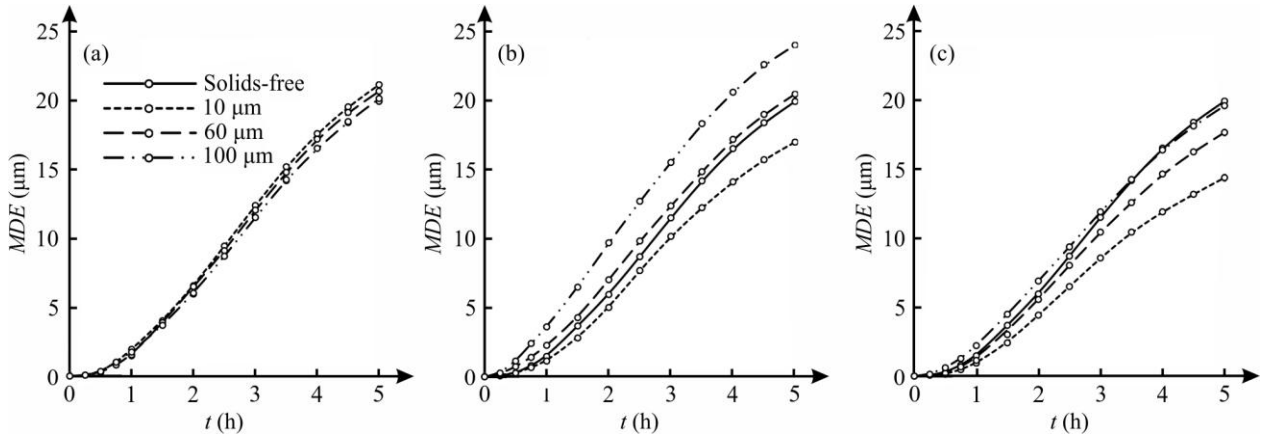

Figure 4. Variation of *MDE* with *t* for different particle sizes at (a) φ_p = 0.005, (b) φ_p = 0.05 and (c) φ_p = 0.2

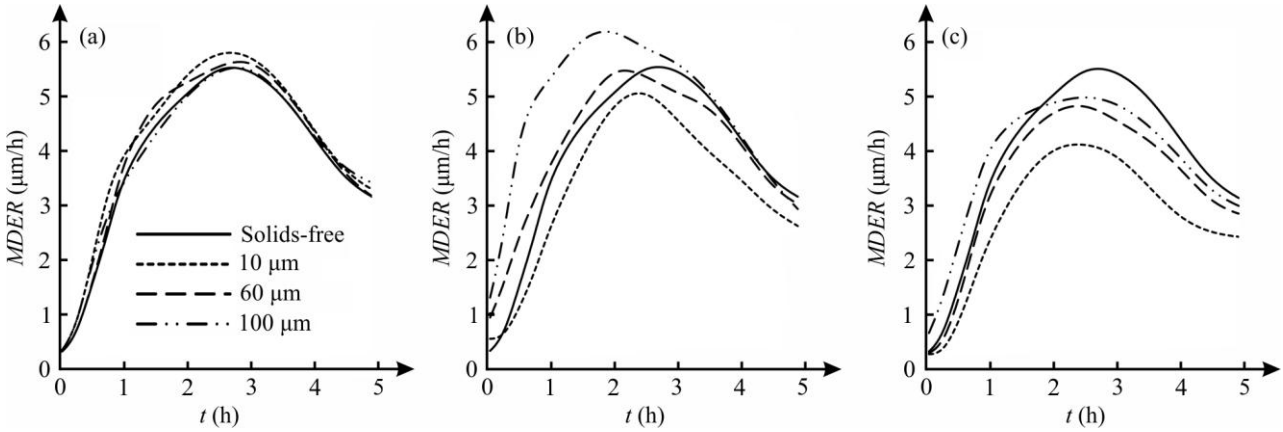

Figure 5. Variation of *MDER* with *t* for different particle sizes at (a) φ_p = 0.005, (b) φ_p = 0. 05 and (c) φ_p = 0.2

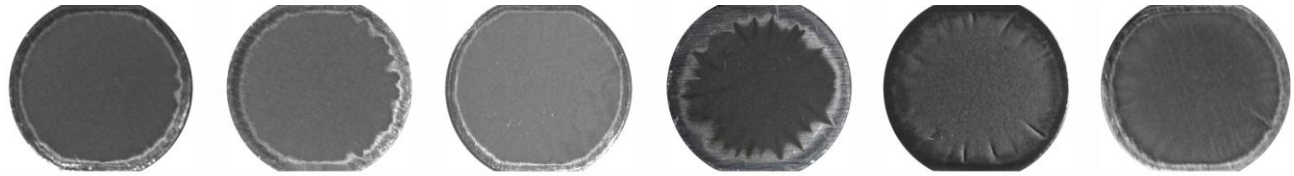

(a) 10 μm, 0.005 v/v (b) 10 μm, 0.05 v/v (c) 10 μm, 0.2 v/v (d) 100 μm, 0.005 v/v (e) 100 μm, 0.05 v/v (f) 100 μm, 0.2 v/v

Figure 6. Pitted surfaces of representative test specimens

Figs. 4 and 5 show the curves of *MDE* and *MDER* versus time for suspensions of small, medium or large SiO_2 particles (10 μm, 60 μm or 100 μm) at low, medium or high concentrations (0.005 v/v, 0.05 v/v or 0.2 v/v), with solids-free case data also plotted for comparison. The macromorphology of representative specimens' eroded surface after an exposure of 300 min for some cases is given in Fig. 6.

When φ_p is at a low level (0.005 v/v), it can be observed from Figs. 4a and 5a that the addition of solid particles invariably leads to more severe erosion (MDE_{5h} = 20.1-21.1 μm) with slightly higher erosion rates ($MDER_{max}$ = 5.4-5.7 μm/h) than in solids-free oil. The difference in curves appears marginal among various particle sizes, though larger particles may result in somewhat lower *MDE* and *MDER* values. In the case of large particles (100 μm) the uneroded area near the edge of the specimen surface (Fig. 6d) is quite similar to that in the solids-free case (Fig. 3b); for small particles (10 μm), by contrast, radial craters become relatively deep and adjacent to the edge (Fig. 6a), narrowing the undamaged outer region.

As for the transformer oil with φ_p = 0.05 v/v SiO_2 particles, small particles (10 μm) alleviate erosion (MDE_{5h} = 17.0 μm) while larger ones, especially those of 100 μm in diameter (MDE_{5h} = 24.0 μm, $MDER_{max}$ = 5.9 μm/h), aggravate material removal (Fig. 4b) and contribute to higher erosion rates (Fig. 5b). It would also appear that adding adequate solid particles can give rise to an earlier maximum-rate period in comparison with the solids-free case, and the larger the particles, the earlier the MP. During the DP, however, mixtures with SiO_2 particles except small ones (60 μm and 100 μm) show similarity in *MDER* curves, virtually coinciding with the solids-free case. As for larger solid particles, CE_P becomes more intense with deeper craters (Fig. 6e),

while for small particles (10 μm) pitting becomes uniformly and lightly distributed over the specimen surface (Fig. 6b).

Under high φ_p conditions (0.2 v/v), CE_P at t = 300 min and erosion rates are reduced by adding particles of all three sizes (MDE_{5h} = 14.4-19.6 μm, $MDER_{max}$ = 4.0-4.8 μm/h); the smaller the particles, the less the erosion and erosion rates (Figs. 4c and 5c). Interestingly, in terms of large particles (100 μm) the erosion rate is higher than that of the solids-free case for the first two hours, and the erosion begins to fall below that of the solids-free case after the end of the fourth hour. Photographs of test specimen surface indicate that radial craters become no longer deep and cavitation pitting is far less severe at exceptionally high concentrations of solid particles, large and small (Fig. 6c and f).

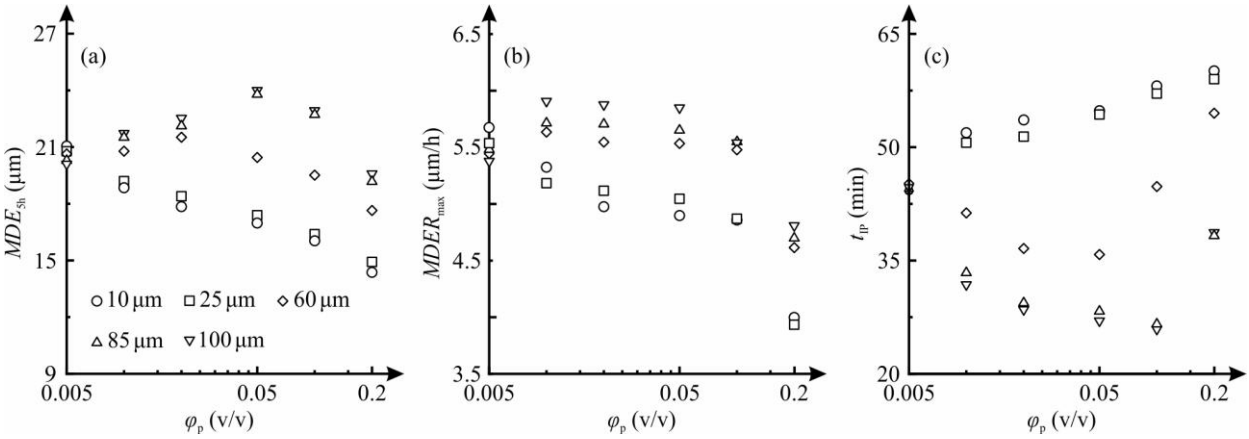

Figure 7. (a) *MDE* at 5 h, (b) $MDER_{max}$ and (c) time to 1 μm for various sizes and concentrations

Fig. 7 illustrates the variation of MDE_{5h}, $MDER_{max}$ and IP duration (t_{IP}) with all six particle concentrations (0.005-0.2 v/v) as regards five particle sizes in the range of 10-100 μm. SiO_2 particles smaller in size (10 μm and 25 μm) show similarity between curves, and so do larger ones (85 μm and 100 μm), with which medium-sized particles (60 μm) bear more resemblance. For small particles (10 μm), erosive wear is becoming less severe (a 31.8% decrease in MDE_{5h}) accompanied with a prolonged IP (15 min longer) as the concentration is elevated from 0.005-0.2 v/v, while for large SiO_2 particles (100 μm), MDE_{5h} gets raised from low to moderate concentrations (below 0.05 v/v) and is then reduced when the concentration becomes high (above 0.1 v/v), resembling the change in t_{IP} which, in contrast, tends to first decrease and then increase. $MDER_{max}$ for all particle sizes remain relatively constant (despite a slight decrease) in the concentration range of 0.01-0.1 v/v, and begin to plunge at high particle concentrations. As for low concentrations (0.005 v/v), however, there is little difference in MDE_{5h}, $MDER_{max}$ and t_{IP} among different particle sizes.

3.3 Possible mechanisms of CE_P

For relatively small SiO_2 particles in the concentration range of 0.01–0.1 v/v, adding SiO_2 particles can lead to less erosion due to the rise in the viscosity of suspensions, which increases with increasing concentration and decreasing size. For relatively large SiO_2 particles with the concentration ranging from 0.01 v/v to 0.1 v/v, the erosion is mainly dependent on the impingement of particles propelled by the bubble wall (Fig. 8a) or micro-jets (Fig. 8b).

At low concentrations (0.005 v/v), erosive wear is more severe than in the solids-free case as a result of the addition of gas/vapor nuclei. Smaller SiO_2 particles contribute to more material removal due to lower energy barriers and larger surface area. In contrast, erosion is alleviated in concentrated suspensions (0.2 v/v) because of the shielding effect of SiO_2 particles (Fig. 8c).

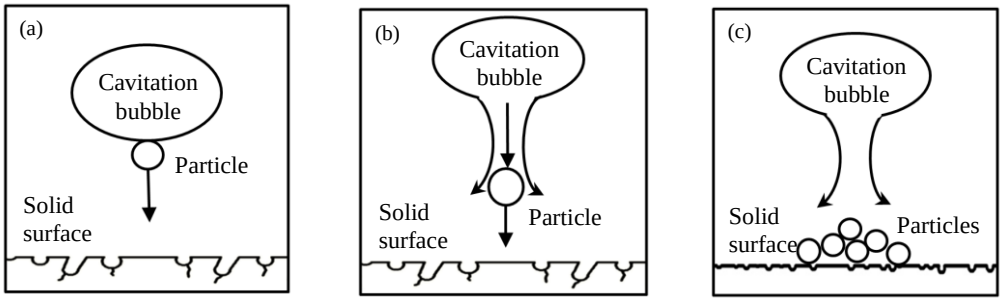

Figure 8. (a) Bubble-wall propulsion, (b) micro-jet propulsion and (c) shielding effect of solid particles

4. CONCLUSIONS

In summary, we have taken particle size and concentration into account to determine whether the addition of SiO_2 particles in the diameter range of 10-100 μm and the concentration range of 0.005-0.2 v/v will alleviate or aggravate CE_P. The results reveal that CE_P gets aggravated at very low concentrations and gets alleviated at very high concentrations; at moderate concentrations, large particles aggravate CE_P while small ones alleviate.

ACKNOWLEDGMENTS

This research was funded by the National Natural Science Foundation of China (Grant No. 51409187), the Fundamental Research Funds for the Central Universities (Grant No. 2019B70914), Postgraduate Research & Practice Innovation Program of Jiangsu Province (Grant No. SJKY19_0482), and Innovation and Entrepreneurship Training Program for College Students (Grant No. 201910294008Z).

REFERENCES

Borkent, B. M., Arora, M., Ohl, C. D., Jong, N. D., Versluis, M., Lohse, D., Morch, K. A., Klaseboer, E. and Khoo, B. C. (2008). The acceleration of solid particles subjected to cavitation nucleation. *Journal of Fluid Mechanics*, 610:157-182.

Chen, H. S., Liu, S. H., Wang, J. D. and Chen, D. R. (2007). Study on effect of microparticle's size on cavitation erosion in solid–liquid system. *Journal of Applied Physics*, 101:103510.

Chen, H. S., Wang, J. D. and Chen, D. R. (2009). Cavitation damages on solid surfaces in suspensions containing spherical and irregular microparticles. *Wear*, 266:345-348.

Einstein, A. (1906). Eine neue bestimmung der molekuldimensionen. *Annals of Physics*, 19:289-306.

Gou, W. J., Wu, J. H., Zhang, H. and Lian, J. J. (2018). Simulation modeling of the combined damage caused by cavitation and abrasion in sediment-laden liquids. *Journal of Fluids Engineering - Transactions of the ASME*, 140:111302.

Gou, W. J., Zhang, H., Li, H. P., Liu, F. and Lian, J. J. (2018). Effects of silica sand on synergistic erosion caused by cavitation, abrasion, and corrosion. *Wear*, 412-413:120-126.

Harvey, E. N., Barnes, D. K., Mcelroy, W. D., Whiteley, A. H., Pease, D. C. and Cooper, K.W. (1944). Bubble formation in animals: I. Physical factors. *Journal of Cellular and Comparative Physiology*, 24:1-22.

Hou, G. L., Ren, Y., Zhang, X. L., Dong, F. X., An, Y. L., Zhao, X. Q., Zhou, H. D. and Chen, J. M. (2020). Cavitation erosion mechanisms in Co-based coatings exposed to seawater. *Ultrasonics Sonochemistry*, 60:104799.

Hu, H. X. and Zheng, Y. G. (2017). The effect of sand particle concentrations on the vibratory cavitation erosion. *Wear*, 384-385:95-105.

Krieger, I. M. and Dougherty, T. J. (1959). A mechanism for non-Newtonian flow in suspensions of rigid spheres. *Transactions of the Society of Rheology*, 3:137-152.

Lian, J. J., Gou, W. J., Li, H. P. and Zhang, H. (2018). Effect of sediment size on damage caused by cavitation erosion and abrasive wear in sediment–water mixture. *Wear*. 398-399:201-208.

Lu, Y. F., Riyanto, N. and Weavers, L. K. (2002). Sonolysis of synthetic sediment particles: Particle characteristics affecting particle dissolution and size reduction. *Ultrasonics Sonochemistry*, 9:181-188.

Mercantili, L., Davis, F., Collyer, S. D. and Higson, S. P. J. (2015). Ultrasonic modification of the viscosity of vegetable, mineral and synthetic oils - Effects of nucleating agents and free-radical scavengers. *Lubrication Science*, 27:177-191.

Mueller, S., Llewellin, W. E. and Mader, H. M. (2010). The rheology of suspensions of solid particles. *Proceedings of The Royal Society, Ser. A: Mathematical Physical and Engineering Sciences*, 466:1201-1228.

Ohl, C. D., Arora, M. and Morch, K. A. (2004). Cavitation inception on micro-particles: A self-propelled particle accelerator. *Physical Review Letters*, 92:174501.

Romero, R., Teran, L. A., Coronado, J. J., Ladino, J. A. and Rodr ǵuez, S. A. (2019). Synergy between cavitation and solid particle erosion in an ultrasonic tribometer. *Wear*, 428-429:395-403.

Stella, J. and Alcivar, R. (2019). Influence of addition of microsized alumina particles on material damage induced by vibratory cavitation erosion. *Wear*, 436-437:203027.

Stoian, D., Eshtiaghi, N., Wu, J. and Parthasarathy, R. (2018). Intensification of sonochemical reactions in solid-liquid systems under fully suspended condition. *Chemical Engineering and Processing: Process Intensification*, 123:34-44.

Teran, L. A., Lain, S., Jung, S. and Rodriguez, S. A. (2019). Surface damage caused by the interaction of particles and a spark-generated bubble near a solid wall. *Wear*, 438-439:203076.

Wang, Y., Wu, J. H. and Ma, F. (2018). Cavitation–silt erosion in sand suspensions. *Journal of Mechanical Science and Technology*, 32:5697-5702.

Wu, J. H. and Gou, W. J. (2013). Critical size effect of sand particles on cavitation damage. *Journal of Hydrodynamics*, 25:165-166.

Wu, J. H., Su, K. P., Wang, Y. and Gou, W. J. (2017). Effect of air bubble size on cavitation erosion reduction. *Science China Technological Sciences*, 60:523-528.

Zhang, Y. N., Qian, Z. D., Ji, B. and Wu, Y. L. (2016). A review of microscopic interactions between cavitation bubbles and particles in silt-laden flow. *Renewable & Sustainable Energy Reviews*, 56:303-318.

Zwietering, T. N. (1958). Suspending of solid particles in liquid by agitators. *Chemical Engineering Science*, 8:244-253.